Crucial roles of charged saccharide moieties in survival of gram negative bacteria against protamine revealed by combination of grazing incidence x-ray structural characterizations and Monte Carlo simulations

Rafael G. Oliveira,[1,2] Emanuel Schneck,[1,3] Bonnie E. Quinn,[4,5] Oleg V. Konovalov,[6] Klaus Brandenburg,[7] Thomas Gutsmann,[7] Tom Gill,[5,8] Charles B. Hanna,[5,9] David A. Pink,[4,5,*,†] and Motomu Tanaka[1,3,5,*,‡]

[1]*Biophysics Laboratory E22, Technical University Munich, D85748 Garching, Germany*

[2]*CIQUIBIC (CONICET)–Departamento de Química Biológica, Facultad de Ciencias Químicas (UNC), Ciudad Universitaria, X5000HUA Córdoba, Argentina*

[3]*Institute of Physical Chemistry and BIOQUANT, University of Heidelberg, D69120 Heidelberg, Germany*

[4]*Department of Physics, St. Francis Xavier University, Antigonish, Nova Scotia, Canada B2G 2W5*

[5]*Advanced Foods and Materials Network of Centres of Excellence, Ontario, Canada K1A 1H5*

[6]*European Synchrotron Radiation Facility (ESRF), 38053 Grenoble, Cedex 9, France*

[7]*Research Center Borstel, D23845 Borstel, Germany*

[8]*Institute of Fisheries Technology, Dalhousie University, Halifax, Nova Scotia, Canada B3J 2X4*

[9]*Department of Physics, Boise State University, Boise, Idaho 83725-1570, USA*

(Received 8 June 2009; revised manuscript received 9 December 2009; published 2 April 2010)

Grazing incidence x-ray scattering techniques and Monte Carlo (MC) simulations are combined to reveal the influence of molecular structure (genetic mutation) and divalent cations on the survival of gram negative bacteria against cationic peptides such as protamine. The former yields detailed structures of bacterial lipopolysaccharide (LPS) membranes with minimized radiation damages, while the minimal computer model based on the linearized Poisson-Boltzmann theory allows for the simulation of conformational changes of macromolecules (LPSs and peptides) that occur in the time scale of ms. The complementary combination of the structural characterizations and MC simulation demonstrates that the condensations of divalent ions (Ca^{2+} or Mg^{2+}) in the negatively charged core saccharides are crucial for bacterial survival.

DOI: 10.1103/PhysRevE.81.041901 PACS number(s): 87.15.kt, 87.10.Rt, 61.05.cf, 61.05.cp

I. INTRODUCTION

The outer surface of gram negative bacteria displays a dense layer of saccharide chains connected to lipids, called lipopolysaccharides (LPSs). An LPS molecule consists of lipid A (the fundamental building block with two phosphorylated *N*-acetylglucosamine units and six hydrocarbon chains), R oligosaccharide unit (core), and O-side chain (polydisperse polysaccharide chain). The core comprises (a) the inner core of four negatively charged saccharide units—two 2-keto-3-deoxyoctonoic acid (Kdo) units and two phosphorylated heptose units—and (b) the outer core of five uncharged saccharides [1]. LPSs stabilize the structural integrity of bacteria and serve as a protective layer against chemical attacks. LPSs are also known as endotoxins since they induce a strong immune response in macrophages by binding to the receptor complex that promotes the secretion of proinflammatory cytokines.

Since the removal or mutation of LPSs is known to result in the death of gram negative bacteria, LPSs are supposed to play crucial roles in the survival of bacteria against antimicrobial peptides. This finding inspires the design of various antibacterial compounds that primarily target LPSs. For example, cationic antimicrobial peptides (CAPs) have been drawing an increasing attention in food industry and medical sciences as antimicrobial alternatives to chemical food preservatives and commonly used antibiotics [2]. Protamine is a cationic peptide (pI=10–12) extracted from the sperm cells of vertebrates and has been used as a food preservative in Japan. To date, many *in vivo* studies demonstrated that divalent cations (Ca^{2+} and Mg^{2+}) significantly increase the minimum inhibitory concentration (MIC) of protamine, which can be used as an indicator for the survival rate of bacteria. It has been suggested that electrostatic interactions are responsible for the interaction of the positively charged protamine molecules with the negatively charged LPS headgroups [3–5].

In general, the outer surfaces of bacteria exposing LPSs can be considered as charged polymer brushes grafted on planar surfaces. After the general framework proposed by Pincus [6], theories of intrinsically flexible polyelectrolyte brushes have been developed by many groups [7–12]. As an alternative approach, atomic-scale molecular dynamics was employed to take the more complex molecular chemistry into account. For example, Kotra *et al.* [13] used a monolayer of 16 LPS molecules that have O-side chains composed of either two or five trisaccharide repeat units. The system included 64 Mg^{2+} ions to account for the influence of divalent cations, and the simulation was run for 200 ps at $T=300$ K. More recently, Lins and Straatsma [14] modeled an asymmetric outer membrane of more complex LPSs of *Pseudomonas aeruginosa* (PAO1) consisting of 16 LPS molecules in the outer leaflet and 40 phosphatidylethanolamine molecules in the inner leaflet, and 3080 SPC/E water molecules containing 104 Ca^{2+} ions. Isothermal-isobaric simulations were initialized for 200 ps and run for 1 ns. In a subsequent account [15], they studied the distribution and

*Corresponding author.
†dpink@stfx.ca
‡tanaka@uni-heidelberg.de

dynamics of Ca^{2+} and saccharide moieties over an elapsed time of 1 ns. These three papers reported the following: (i) Ca^{2+} ions are essential for the stability of the LPS membranes [13,15]; (ii) most of the Ca^{2+} ions are confined within a thin layer (thickness of ~2 nm) in the inner core [14]; (iii) a well-defined structural pattern existed for the location of the Ca^{2+} ions interacting with the inner core phosphate groups [14,15]; and (iv) water penetrated the membrane to a depth of ~3 nm [15].

Previously, we created a "minimum computer model" using linearized Poisson-Boltzmann theory in order to calculate the number density profiles of different ion species, saccharide units, and cationic peptides by Monte Carlo (MC) simulations [16]. This model enabled us to simulate the conformational changes of molecules on the time scales of $>10^{-3}$ s in a large simulation volume containing 100 PAO1 LPS molecules in the xy plane and $0 \leq z \leq 200$ Å. The simulations predicted that CAPs are kept away from the membrane surface in the presence of divalent ions, resulting in an increase in the MIC [16]. More recently, we carried out grazing incidence diffuse x-ray scattering out of the specular (GIXOS) plane on the monolayer of LPS molecules from a rough mutant, *Salmonella enterica* Minnesota R60, at the air/water interface [17]. GIXOS at the air/water interface [18] offers a unique advantage over the specular reflectivity technique by significantly reducing the irradiation time (by a factor of 100) and thus minimizing the radiation damage to biological samples. From the quantitative reconstruction of electron density profiles normal to the membrane surface, we demonstrated the collapse of carbohydrate chains in the presence of Ca^{2+} ions and the interaction of protamine molecules with the LPS membranes, which is consistent with the MC simulation results.

In the present paper, we extend this strategy to study the influence of the genetic modification of molecular structures. Here, we deal with a rough mutant LPS from *Escherichia coli* strain F515 (LPS Re) that consists of lipid A (with two phosphorylated *N*-acetylglucosamine units and six hydrocarbon chains) and two Kdo units [19]. This LPS is the shortest LPS unit required for the survival of bacteria [19,20]. LPS Re molecules are spread on buffer subphase with and without Ca^{2+} and form insoluble (Langmuir-type) monolayers at the air/water interface. Similar to our previous report, we calculate the vertical electron density profiles from GIXOS signals, which can be compared directly with the MC simulations based on the minimal computer model. In this study, we additionally carry out grazing incidence (wide-angle) x-ray diffraction (GIXD) [21,22] to detect the lateral structural ordering of hydrocarbon chains in pure LPS Re monolayers. To evaluate the chain ordering by MC simulations, we introduce a two-state model [23–26] that assumes a chain to be either in an ordered (ground) state or in a disordered (excited) state.

The use of purified LPSs with monodisperse short oligosaccharide headgroups enables us to study the cooperative molecular interactions under well-defined thermodynamic conditions, as well as to approximate the system as a set of distinct slabs with defined electron density, thickness, and interface roughness (slab model). To study the impact of protamine on the monolayer structures in the presence and absence of Ca^{2+}, we inject protamine from herring into the subphase at a constant lateral density of LPS molecules. The interaction of protamine and LPS Re is tracked by monitoring the change in surface pressure and the scattering and diffraction signals.

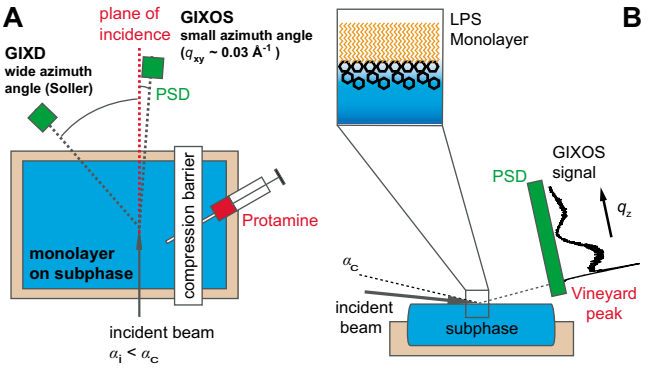

FIG. 1. (Color online) Schematic illustrations of grazing incidence x-ray scattering setup on the Langmuir film balance: (A) top view and (B) side view.

At the final stage, to clarify if the Kdo units are essential for the survival against protamine, we also monitor the interaction of protamine with a monolayer of lipid A, which is prepared by acid hydrolysis of the same LPS Re [27]. Details on the experimental results and simulations are discussed in the following sections.

II. MATERIALS AND METHODS

A. Sample preparation

Deep rough mutant LPS (LPS Re) was extracted from *E. coli* strain F515, and the purified sample was lyophilized as reported [19,20]. MALDI-TOF mass spectrometry shows a sharp peak at 1797 Daltons, corresponding to the molecular weight of the lipid A portion with its hexaacyl lipid anchor plus a peak at 2236 for the whole molecule. Herring protamine was isolated by HCl digestion and washed extensively with distilled de-ionized water on a 1000 Da molecular weight cutoff filter [28]. Pressure-area isotherms were recorded with a Langmuir film balance (Kibron, Inc., Finland). The stock solution of LPS Re (1 mg ml^{-1} in $CHCl_3/CH_3OH=9/1$ in v/v) was spread on the subphase. After the evaporation of the solvent, the film was compressed at a constant speed of 1–10 Å^2/molecule min. To study the influence of Ca^{2+} ions, we used two types of buffer subphases (pH 7.4): (i) "Ca^{2+}-free" buffer that consists of 5 mM Hepes and 100 mM NaCl and (ii) "Ca^{2+}-loaded" buffer that additionally contains 50 mM $CaCl_2$.

B. Grazing-incidence x-ray scattering

GIXOS and GIXD measurements (Fig. 1) are conducted at ID10B beamline of the European Synchrotron Radiation Facility (ESRF), Grenoble [29]. The LPS monolayer deposited on a homemade Langmuir film balance is kept in He atmosphere to minimize the radiation damage. The monochromatic beam ($\lambda=1.54$ Å) illuminates the monolayer at an

incident angle (α_i=0.11°) slightly below the critical angle of the air/water interface (α_c=0.152°). The penetration depth of the evanescent wave Λ is a function of the angle of incidence α_i [30],

$$\Lambda \cong \frac{1}{q_c}\sqrt{\frac{\alpha_c^2}{\alpha_c^2 - \alpha_i^2}},$$

where q_c is the momentum transfer at the critical angle α_c, $q_c=(4\pi/\lambda)\sin\alpha_c$.

GIXD measures the diffraction from the quasi-two-dimensional ordering of hydrocarbon chains at relatively wide angles and thus can reveal the interchain characteristic distances, the degree of lattice distortion from the ideal hexagonal packing, and the tilt angle of hydrocarbon chains to the surface normal [31,32]. In the GIXD setup, the intensity of the scattered beam is collected with a position sensitive linear detector perpendicular to the monolayer surface at variable azimuth angle (δ). We use additionally a Soller collimator (with an angular resolution of 0.05°) to improve the counting statistics.

In the GIXOS measurements, the intensity of the scattered beam is collected with a position sensitive linear detector perpendicular to the monolayer surface at a fixed small azimuth angle ($q_x \sim 0.029$ Å^{-1}). In case in-plane momentum transfer is very small ($q_{xy} \sim 0$) and interface roughness is conformal, the measured diffuse intensity is connected to the corresponding reflectivity curve [18]

$$I(q_z) \propto |T(k_{in})|^2 |T(k_{out})|^2 \frac{R(q_z)}{R_F(q_z)}. \quad (1)$$

Here, $I(q_z)$ denotes the intensity measured in a GIXOS experiment, $R(q_z)$ is the corresponding specular reflectivity as measured in a θ-2θ scan, $R_F(q_z)$ denotes the specular reflectivity from a flat (ideal) surface, and $T(k_i)$ and $T(k_{out})$ represent the characteristic Vineyard functions for the grazing incidence configuration. The data are fitted using a self-developed routine based on the master formula for specular reflectivity,

$$R(q_z) = R_F(q_z)\left|\frac{1}{\rho}\int \frac{d\rho(z)}{dz}\exp(iq_z z)dz\right|^2. \quad (2)$$

Note that the data points below q_z=0.06 Å^{-1} are not included in the fit because the master formula loses its validity for low q_z.

III. THEORETICAL MODELING

A. Minimal model

The interactions that distinguish between the various moieties of the Kdo core are electrostatic and hydrogen bonding. Because each LPS molecule possesses six hydrocarbon chains, the average distance between the charged core segments ranges between 12 and 14 Å. The charged membrane surface cannot be represented by a continuum since the charge distribution is neither uniform nor static, which can lead to significant fluctuations in the local charge density. Accordingly, the commonly used DLVO theory [33] would be inadequate [34,35]. Although a mean-field Poisson-Boltzmann theory [33] can be a satisfactory model of an aqueous solution of monovalent ions, it is inadequate for modeling multivalent ions in a polyelectrolyte [36] since they can take part in bridging that can exhibit a high degree of three-body correlations. If one considers the complexity of the system and thermal fluctuations of the charge density, it is reasonable to set the resolutions of our computer simulation to be ~2 Å. Following our previous accounts [16,17], our model system has 100 close-packed LPS Re molecules in the plane of the membrane, the xy plane. One of the major advantages of our approaches is to monitor the conformational change of molecules occurring on the time scale of $>10^{-3}$ s.

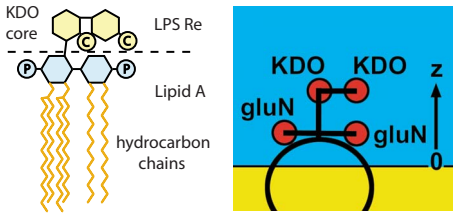

FIG. 2. (Color online) Structure (left) and minimal model (right) of the LPS from *Escherichia coli* strain F515 (LPS Re) used in this study. LPS Re consists of two Kdo sugars and lipid A that can be obtained by the hydrolysis of LPS Re. P and C in the chemical structure (left) indicate negatively charged phosphate and carboxylate groups, respectively. The four filled spheres in the model (right) represent negatively charged saccharides. The upper and lower regions separated at z=0 coincide with the water and hydrocarbon regions, respectively.

B. LPS and protamine

Each charged monosaccharide is represented by a sphere of radius r_{sug}, with the electric charge located at its center, and connected to each other by bonds of equilibrium length L_0. Figure 2 shows the schematic structures (left) and the minimal model (right) of an LPS from *Escherichia coli* strain F515 (LPS Re) and its hydrolyzed product, lipid A. The charged sugar groups are represented by filled spheres, and the relative angles between the bonds connecting the sugar spheres were described elsewhere [16,17]. The plane z=0 defines the boundary between the water ($z>0$) region occupied by C═O and N—H groups and the hydrocarbon chain ($z<0$) region. The hydrocarbon chains serve to anchor the hydrophilic groups in the membrane and are represented as a sphere with a radius of R_{anchor}, which is determined by the cross-sectional area of the hydrocarbon chain region projected to the membrane surface (Appendix). To take into account flexibility of the hydrocarbon chain region, we permitted the anchoring sphere to rotate around its center [16,17]. The sugar spheres are allowed to move according to the bond-stretching technique [16,37,38], the angle between successive bonds α being permitted a slight variation $\pm\Delta\alpha$. In this study, we use the same minimal model of protamine as the one we previously reported [16], and the positions of all protamine spheres were confined to the water region ($z>0$).

C. Solvent

We use a continuum dielectric model with monovalent ion screening represented by linearized Poisson-Boltzmann theory [33,36,39–41]. This approximation is valid for classical bulk electrostatics on a spatial resolution of ~2 Å [42] though it is unlikely to describe "bound" water near a surface. Hydrated ions (Ca^{2+}, Na^{+}, and Cl^{-}) are represented by spheres with the charges located at their centers. All Ca^{2+} and their associated Cl^{-} ions are explicitly represented in this way, but approximately half of the associated monovalent ion pairs (Na^{+} and Cl^{-}) are represented by a Debye screening length, κ^{-1}. If the remainder of the monovalent ions give rise to an effective screening length, κ_1^{-1}, then the total effective screening length is $\kappa_{tot}^{-1} \approx 10$ Å, corresponding to ~100 mM monovalent salts, where $\kappa_{tot}^2 = \kappa^2 + \kappa_1^2$.

D. Electrostatic interactions

The aqueous solution and the hydrocarbon-chain region of an LPS monolayer were represented by two dielectric continua separated by a plane at $z=0$ with relative permittivities of $\varepsilon_w = 81$ and $\varepsilon_{hp} = 5$, respectively [33,40]. We calculate the electric potential at a point $\vec{R} = x\hat{x} + y\hat{y} + z\hat{z}$ in the aqueous solution containing monovalent salt in the presence of an electric charge Q located at $\vec{R}_0 = x_0\hat{x} + y_0\hat{y} + z_0\hat{z}$. Here $\hat{x}$, $\hat{y}$, and $\hat{z}$ are unit vectors with $\hat{z}$ perpendicular to the plane of the membrane/water interface. Netz [43] (see also Netz and Andelman [44] and Fleck *et al.* [39]) derived expressions for the electrical potential at $\vec{R}$ [43]. Since $\eta = \varepsilon_{hp}/\varepsilon_w \approx 0.06$ and $\chi = (1-\eta)/(1+\eta)$, the expression for the potential simplifies [43]. The electrical potential at $\vec{R}$ becomes

$$V(Q, \vec{R}_0, \vec{R}) = (1/4\pi\varepsilon_w\varepsilon_0) \sum_j Q_j f(|\vec{R}_j|),$$

$$f(|\vec{R}_j|) = e^{-\kappa|\vec{R}_j|}/\vec{R}_j, \tag{3}$$

where the sum is over $j = 1-2$, $\vec{R}_1 = \vec{R} - \vec{R}_0$, $\vec{R}_2 = \vec{R} - \vec{R}_0 + 2z_0\hat{z}$, $Q_1 = Q$, and $Q_2 = \chi Q$. Potential (3) goes to the two correct limiting values as $\varepsilon_{hp} \to 0$ or as $\kappa \to 0$.

E. Hydrogen bonding

A sugar sphere is allowed to form a hydrogen bond of energy 0.4×10^{-20} J with a neighboring sugar sphere if the spheres are sufficiently closer than 3 Å. The interaction is not directional, but sugar spheres possess hard-core repulsive interactions with each other so that such model hydrogen bonds are distributed over the sugar surfaces.

F. Ordering of hydrocarbon chains

We modeled the phase transition of an LPS layer as the temperature changes. We utilize a two-state model [23–26], assuming that the chains are either in an ordered ground state (*S*, "small" cross-sectional area) or in a disordered excited state (*B*, "big" cross-sectional area). We deduced hydrocarbon chain cross-sectional areas (projected onto the plane of the LPS layer), energies, and degeneracies and chose the strength of the intermolecular interaction, $J_0 = 0.300 \times 10^{-20}$ J, to yield a phase transition temperature of ~314 K [Fig. 5(A)]. This corresponds approximately with the observed phase transition of LPS Re at around 300–320 K (303 K for Re and 319 K for lipid A). Since the intent of this model is to see the effect of Ca^{2+} ions upon the phase transition, we considered it unnecessary to fine tune J_0. The details of deriving the properties of states *S* and *B* are given in the Appendix.

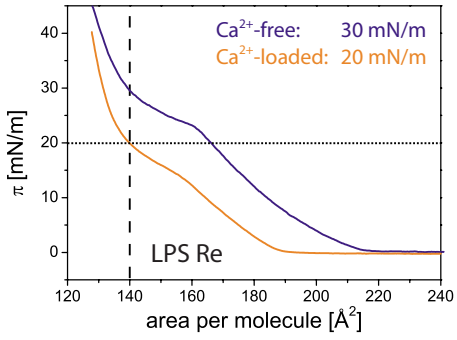

FIG. 3. (Color online) Pressure-area isotherms of LPS Re monolayers on Ca^{2+}-free subphase (dark) and Ca^{2+}-loaded subphase (bright). Grazing-incidence x-ray structural characterizations and protamine adsorption experiments (see below) are carried out at a constant surface pressure ($\pi = 20$ mN m^{-1}; dotted line) or at a constant area per molecule ($A = 140$ Å^2; broken line).

G. Computer simulation

Our MC simulations employed the Metropolis algorithm [45,46] and periodic boundary conditions along the *x* and *y* axes. At each MC step, we attempted to change the positions of sugar spheres and ions. To take the constrained molecular flexibility into account, we restrict the relative angle between *z* axis and the bond connecting Kdo cores and the lipid anchor to be 30° ± 5°. For all horizontal bonds shown in Fig. 2, we permit them to make an angle of 30° ± 5° (semiflexible case) with a vector perpendicular to a bisector of the two bonds at their point of connection. Each lipid anchors can vary its position along the *z* axis by ±1.5 Å as well as rotate around its center as long as such motion does not result in the movement of the headgroup moieties into $z < 0$. The *z* dimension of the water region of the simulation volume ranged from $0 \le z \le 200$ Å. For the simulations of all the x-ray scattering experiments, the temperature is kept constant at $T = 300$ K. On the other hand, the thermotropic phase transition of hydrocarbon chains is simulated between 275 and 340 K. Throughout this study, the entire system was equilibrated for $>10^6$ Monte Carlo steps, and the properties of the system were measured for another 10^6 steps.

IV. RESULTS AND DISCUSSION

A. Pressure-area isotherms

Figure 3 represents the pressure-area isotherms of LPS Re monolayers on "Ca^{2+}-free subphase" (dark) and "Ca^{2+}-loaded subphase" (bright). On Ca^{2+}-loaded buffer, the

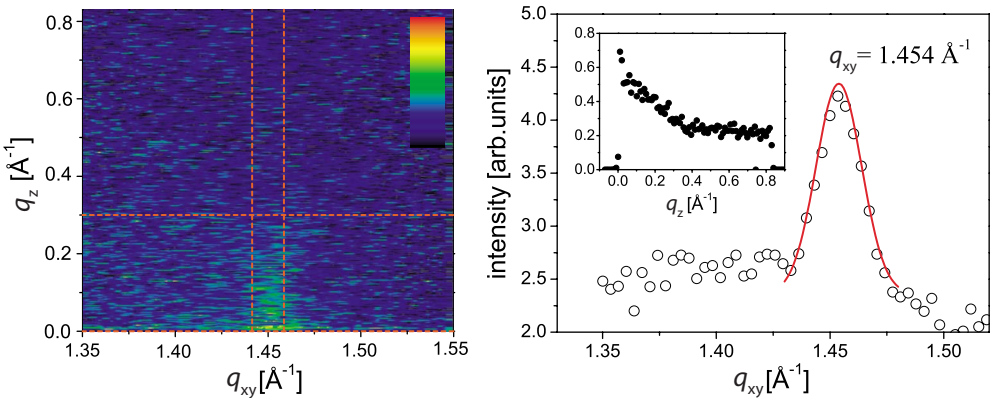

FIG. 4. (Color online) (A) Example of a typical GIXD reciprocal space map of LPS Re monolayers on Ca^{2+}-loaded subphase at $A=140$ Å ($\pi=20$ mN m^{-1}). (B) The measured intensity integrated along q_z plotted as a function of q_{xy} is presented in the main panel, while the intensity integrated along q_{xy} plotted as a function of q_z is presented as an inset. A single peak at $q_z=0$ indicates that hydrocarbon chains take a hexagonal ordering with an upright conformation. On the other hand, no GIXD peak could be observed the absence of Ca^{2+} at $\pi=20$ mN m^{-1} (data not shown), indicating that the presence of Ca^{2+} increases the lateral ordering of hydrocarbon chains. Broken lines indicate the integration limits along each axis.

onset of pressure increase appears at $A\sim185$ Å^2. This value is smaller than that on Ca^{2+}-free buffer ($A\sim215$ Å^2), suggesting that headgroups in Ca^{2+}-loaded buffer are more compact than those in Ca^{2+}-free buffer. On the other hand, when the monolayer is compressed up to the liquid-condensed phase ($A\sim140$ Å^2) the lateral compressibilities of the monolayer calculated from the isotherms are $\chi_{\text{free}}=-(1/A)(\partial A/\partial\pi)\sim0.011$ mN^{-1} m and $\chi_{\text{loaded}}\sim0.013$ mN^{-1} m. The values obtained on the two subphases are similar, implying that the lateral compressibility of the monolayer in a solid phase is governed by that of hydrocarbon chains. The plateaulike regimes observed on both subphases can be interpreted as the coexistence of fluid (liquid-expanded) and solid (liquid-condensed) phases (see Fig. 4 for more details). It should be noted that the shoulder regime appeared at $\pi=25-30$ mN m^{-1} on Ca^{2+}-free subphase, while the corresponding feature is observed at much lower surface pressure ($\pi=15-20$ mN m^{-1}) in the presence of $CaCl_2$. The observed differences in the isotherms suggest that intermolecular interactions between LPS molecules are significantly influenced by the presence of Ca^{2+}.

B. Impact of Ca^{2+} on lateral chain ordering

To detect the lateral ordering of hydrocarbon chains, GIXD experiments are carried out either at a constant surface pressure ($\pi=20$ mN m^{-1}, indicated with a dotted line in Fig. 3) or at a constant area per molecule ($A=140$ Å^2, indicated by a broken line in Fig. 3). Figure 4 shows (A) the measured reciprocal space map (intensity plotted as a function of the out-of-plane and in-plane reciprocal space coordinates q_z and q_{xy}, respectively) and (B) the intensity integrated along q_z plotted as a function of q_{xy} for a LPS Re monolayer, measured on Ca^{2+}-loaded subphase at $\pi=20$ mN m^{-1}. The intensity integrated along q_{xy} plotted as a function of q_z is presented as an inset of Fig. 4(B). The integration ranges for both cases are indicated by broken lines. As shown in Fig. 4, the measured GIXD signal exhibits a single peak whose maximum is located at $q_z=0$. This finding indicates that the hydrocarbon chains of LPS Re molecules take upright conformation with a negligibly small tilt angle with respect to the direction normal to the water surface and form a hexagonal lattice [32]. From the peak position $q_{xy}=1.45$ Å^{-1} (corresponding to the characteristic distance of $w=4.32$ Å), the area per chain of $a=(2/\sqrt{3})w^2=21.5$ Å^2 can be calculated. The area per molecule calculated from the number of chains, $A=129$ Å^2, seems to stay within a reasonable range from the value reported by wide-angle x-ray scattering in dispersions [47] and the area per molecule estimated from the pressure-area isotherm ($A=140$ Å^2). In contrast, in the absence of Ca^{2+}, no GIXD peak can be observed at $\pi=20$ mN m^{-1}. This can be attributed to the fact that the monolayer on Ca^{2+}-free buffer still remains in a fluid, liquid-expanded phase; i.e., there is no lateral ordering of hydrocarbon chains. In fact, a GIXD peak with almost identical features can be observed on Ca^{2+}-free buffer when the film is compressed to $\pi=30$ mN m^{-1}, corresponding to the area per molecule of $A=140$ Å^2 (data not shown).

In order to further consider the influence of Ca^{2+} ions on the lateral ordering of hydrocarbon chains, MC simulations were employed to calculate the probability of finding a molecule to have its hydrocarbon chains in their ordered S state (Appendix) in Ca^{2+}-loaded [Fig. 5(A)] and Ca^{2+}-free [Fig. 5(B)] buffers. The influence of Ca^{2+} ions on the lateral ordering of hydrocarbon chains is evaluated by the thermotropic phase transition upon heating (filled circles) and cooling (open circles) cycles, which is different from the GIXD experiments on the film balance at a constant temperature. Here, the strength of interactions is adjusted to match the phase transition temperature of $T_m\sim314$ K, which is close to the T_m values for LPS Re (303 K) and lipid A (320 K). Note that the T_m is defined as the middle point of the transition region upon heating and cooling, indicated by shaded area in the figure. The presence of Ca^{2+} causes a clear increase in the melting transition upon heating by ~3 K, which is larger than the temperature step (1.5 K). This can be compared to the previous study of Blatt and Vaz [48] that reported the increase in the transition temperature of

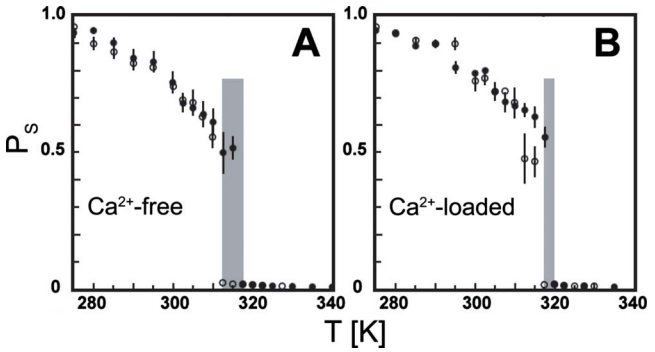

FIG. 5. (Color online) Probability of finding the hydrocarbon chain moiety of an LPS molecule in its ordered (S) state in the (A) absence and (B) presence of Ca^{2+} ions plotted as a function of temperature T. Filled data points indicate averages of 20 heating runs, while the open ones are averages of 20 cooling runs. Vertical bars indicate standard deviations (SDs) over the 20 runs. Where absent, the SDs are less than the size of the data points. Shaded areas indicate the phase transition regions. The limits are defined by the lowest temperatures for the system to be in a fluid ("melted") phase.

dimyristoylphosphatidylcholine membranes by several degrees in the presence of >50 mM of Ca^{2+} ions. A consequence of this is that, at a fixed temperature—for example, 300 K—the probability of finding the hydrocarbon chains in their (ordered) S state increases from ~0.75 (without Ca^{2+}) to ~0.79 (with Ca^{2+}). This suggests that Ca^{2+} also increases the *lateral* ordering of hydrocarbon chains, showing good agreement with the GIXD results. These data are also in agreement to data published on the influence of divalent cations on the aggregate structures of LPS dispersions [49].

C. Impact of Ca^{2+} on vertical structures: Experiments

To determine the vertical structures of LPS Re monolayers in the absence and presence of Ca^{2+}, GIXOS experiments were carried out at a constant area per molecule $A = 140$ Å^2 (indicated by a broken line in Fig. 3). Figure 6(A) shows the measured GIXOS signals from LPS Re monolayers on Ca^{2+}-free (open circles) and Ca^{2+}-loaded (filled circles) subphases. The curves exhibit a clear difference in their global shapes: the more pronounced second maximum ($q_z \sim 0.3$ Å^{-1}) in the presence of Ca^{2+} indicates that Ca^{2+} causes an increase in the electron density contrast. In order to gain deeper insight into this structural change, we modeled the measured GIXOS signals using a two-slab model for the internal monolayer structure: the first slab represents hydrocarbon chains and the second one the carbohydrate headgroups. Each slab possesses a thickness d and a constant electron density ρ. The electron density gradients across the interfaces are modeled with error functions characterized by the transition widths σ. For the fitting, we described the effective electron density profiles at the air/water interfaces as the internal monolayer structures smeared out due to the capillary waves of the water surface with a root mean square transition width of $\sigma = 2$ Å. To exclude unphysical scenarios and to minimize the number of floating parameters, we fixed three parameters (d_1, ρ_1, and σ_1) that determine the structure of the first slab (hydrocarbon chains; see Table I) by referring to the values reported for a lipid monolayer that possesses almost the same chain length and density [50]. On the other hand, the parameters characterizing the structure of the second slab (d_2, ρ_2, σ_2, and σ_3) were allowed to float while fitting to account for changes in the saccharide headgroups. The standard errors of the four floating parameters were determined in the following manner: each parameter was varied stepwise while performing a least-squares fit to the experimental signal for the three other floating parameters. The quality of each fit was assessed using a Monte Carlo bootstrap method [51] under consideration of the experimental errors of the measured GIXOS signals. Here, the confidence band was defined to be one standard deviation. The calculated electron densities, thicknesses, and interface roughness of all the slabs are summarized in Table I. The parameters corresponding to the best matching models indicate that calcium induces an increase in headgroup electron density and/or a reduction in the roughness of the headgroup/water interface. Although the errors of the parameters do not allow us to identify these differences in detail, the obtained results show good consistency with our previous study on monolayers of LPS with longer headgroups [17].

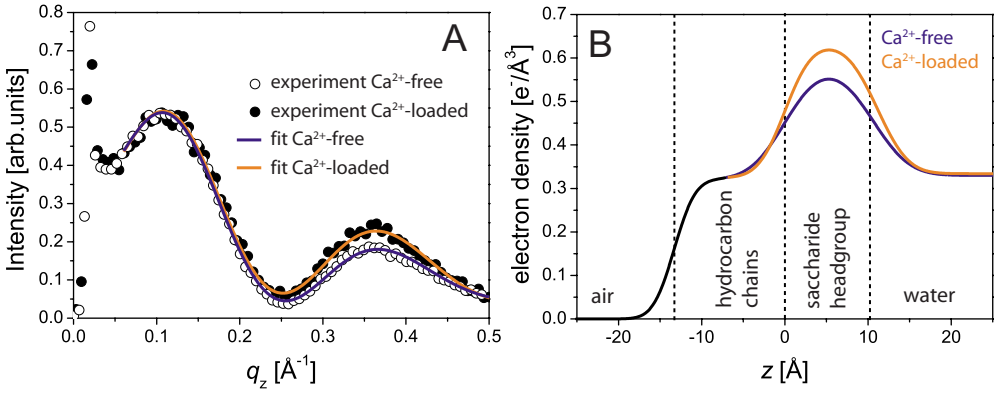

FIG. 6. (Color online) (A) GIXOS raw data from LPS Re monolayers on Ca^{2+}-free subphase (open circles) and Ca^{2+}-loaded subphase (filled circles) at $A = 140$ Å together with the fits (solid lines) corresponding to the best matching model parameters. (B) Internal electron density profiles along z axis (perpendicular to the interface) corresponding to the best matching model parameters.

TABLE I. Electron density ρ, thickness d, and roughness σ corresponding to the least-squares fits of the LPS Re GIXOS data [Fig. 6(A)]. The internal monolayer structure can be described with a two-slab model. Capillary waves were assumed to possess a height standard deviation of $\sigma=2$ Å. Errors of the floating parameters indicate a confidence band of one standard deviation. The electron density profiles reconstructed from the best matching parameters are shown in Fig. 6(B).

LPS Re on Ca^{2+}-free subphase ($\pi=30$ mN m^{-1})			
	ρ (eÅ^{-3})	d (Å)	σ (Å)
Air	0	∞	N/A
Hydrocarbon chain	0.31 (–)	13.3 (–)	2 (–)
Sugar head	0.58 ± 0.12	10.6 ± 0.9	3.3 (>2.5)
Water	0.33 (–)	∞	3.5 ± 1.8
LPS Re on Ca^{2+}-loaded subphase ($\pi=20$ mN m^{-1})			
	ρ (eÅ^{-3})	d (Å)	σ (Å)
Air	0	∞	N/A
Hydrocarbon chain	0.31 (–)	13.3 (–)	2 (–)
Sugar head	0.62 ± 0.08	11.0 ± 0.8	2.9 ± 1.4
Water	0.33 (–)	∞	2.5 ± 1.7

D. Impact of Ca^{2+} on vertical structures: MC simulations

In Fig. 7, we present the number density distributions perpendicular to the interface, $\Phi(z)$, for LPS Re monolayers for (A) Ca^{2+}-free subphase and (B) Ca^{2+}-loaded subphase calculated by MC simulations. The number densities of LPS sugars, ions, and protamine are along z axis. When one compares the results presented in Figs. 7(A) and 7(B), the most pronounced is that the number density of Na^+ ions (Na) in the Kdo core region is significantly suppressed in the presence of Ca^{2+} ions (Ca). Under both conditions, the densities of Cl^- ions are very small near the negatively charged Kdo cores and increase slowly toward the bulk. It should be noted that the change in the number densities of sugars (LPS) is relatively minor probably due to the limited vertical compressibility of small headgroups. However, it is notable that the slight compaction of the headgroups indicated by the MC simulation seems to follow the same tendency as the increase in the lateral chain ordering suggested both from GIXD experiment (Fig. 4) and from MC simulations (Fig. 5). Furthermore, the electron density profiles $\rho(z)$ reconstructed from the number density distributions $\Phi(z)$ presented in Fig. 7(C) show good agreement with those calculated from the GIXOS results [Fig. 6(B)]. It should be noted that the q range available in the x-ray experiments is insufficient to resolve the substructure of the saccharide headgroups as it is seen in the MC simulations, so that the saccharide headgroups were treated as one slab with a constant electron density. Nevertheless, the average electron densities in the saccharide layer ($0<z<10.5$ Å) calculated from the MC simulations, $\rho_{Ca^{2+}\ free}=0.56e/Å^3$ and $\rho_{Ca^{2+}\ loaded}=0.58e/Å^3$, agree well with the electron density values of the saccharide headgroup slab deduced from the GIXOS signals (Table I).

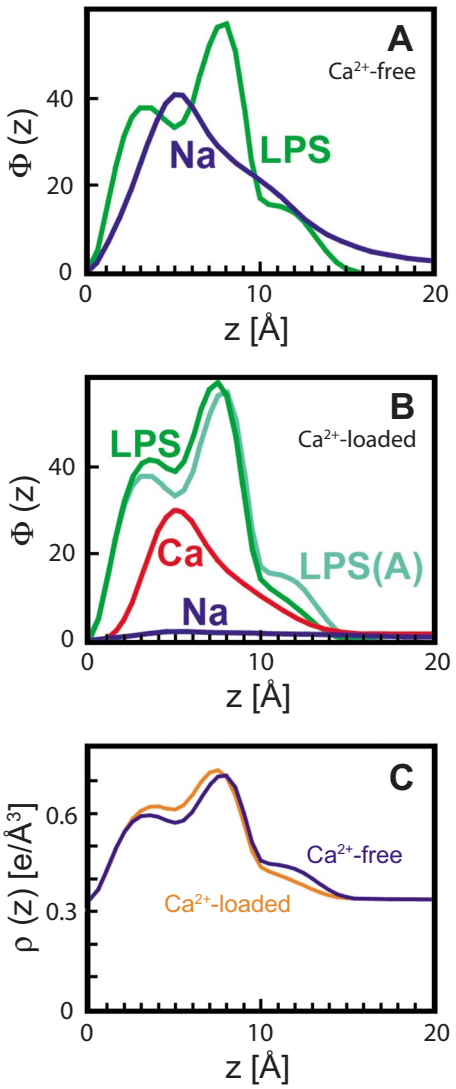

FIG. 7. (Color online) The number densities $\Phi(z)$ of sugar moieties (LPS), Na^+ ions (Na), and Ca^{2+} ions (Ca) for LPS Re monolayers on (A) Ca^{2+}-free subphase and (B) Ca^{2+}-loaded subphase calculated by MC simulations. (A) LPS in panel (B) stands for the LPS density in panel (A) for the direct comparison. (C) The electron density profiles $\rho(z)$ calculated from the number density distribution $\Phi(z)$ agree well with those calculated from the GIXOS results [Fig. 6(B)], with the value at $z=0$ approaching the experimental value of 0.33. The arrow shows the analytically calculated average electron density for a uniform hydrocarbon chain layer.

E. Interaction of LPS Re with protamine

Interactions of LPS Re monolayers with CAPs in the presence and absence of Ca^{2+} are studied upon the injection of herring protamine to the subphase (i.e., beneath the monolayer) at $A=140$ Å^2. The final concentration of protamine in the subphase, 1 mg ml^{-1}, is comparable to the MIC determined by *in vivo* experiments, 1.25 mg ml^{-1} [52]. To ex-

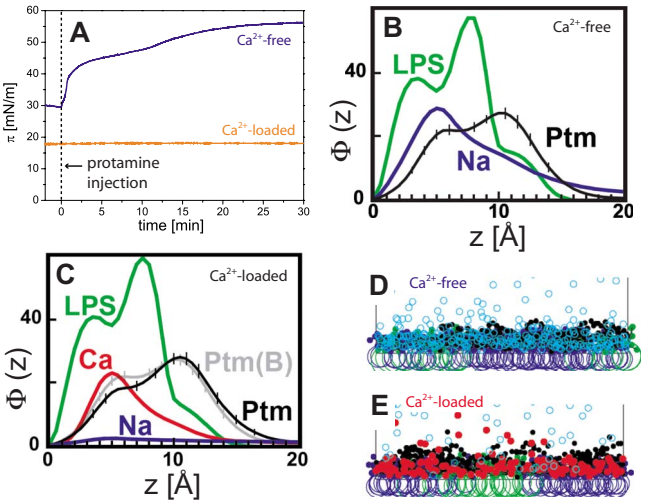

FIG. 8. (Color online) Interaction of protamine with LPS Re monolayers. (A) Surface pressure of LPS Re monolayers plotted as a function of time on Ca^{2+}-free (dark) and Ca^{2+}-loaded (bright) buffers at $A=140$ Å^2. Upon injection of protamine solution at $t=0$ (final concentration of ~ 1 mg ml^{-1}, comparable to the MIC), a significant increase in the surface pressure is observed in the absence of Ca^{2+} ions, indicating the deep penetration of protamine into the LPS Re monolayer. However, the surface pressure stays stable in the presence of Ca^{2+}, which proves that charged Kdo cores are sufficient for bacterial survival against protamine in the presence of Ca^{2+}. Panels (B) and (C) show the number densities $\Phi(z)$ of sugar moieties (LPS), Na^+ ions (Na), and Ca^{2+} ions (Ca) for LPS Re monolayers in the presence of five protamine molecules (Ptm) in the simulation volume. In panel (C), the number density of protamine on Ca^{2+}-free subphase [Ptm(b)] is given for the direct comparison. Panels (D) and (E) show instantaneous side views of the systems in Ca^{2+}-free and Ca^{2+}-loaded buffers, respectively. Na^+ ions are open circles, while Ca^{2+} ions are bright filled circles. In Ca^{2+}-loaded buffer, the loose peptide chain (dark filled circles) termini sticking out to the bulk suggest the weaker interaction of protamine with the LPS Re monolayer.

clude the possibility that the surface activity of protamine permits their direct adsorption to the air/water interface, we confirm that the surface pressures of both buffers containing 1 mg ml^{-1} of protamine remain zero in the absence of LPS Re monolayers, which agrees well with a previous report [53]. Figure 8(A) shows the surface pressures of LPS Re monolayers recorded as a function of time on Ca^{2+}-free (dark) and Ca^{2+}-loaded (bright) buffers. The time point at which the protamine solution is injected is defined as $t=0$ and indicated by a broken line.

In the absence of Ca^{2+} ions (dark), the surface pressure rapidly increases almost up to $\pi \sim 55$ mN m^{-1}. The significant increase in the surface pressure ($\Delta\pi \sim 25$ mN m^{-1}) indicates that protamine goes deeper into the inner core region toward the air/water interface. The GIXD peak is no longer observed after protamine injection, implying that the lateral chain ordering is disrupted by the penetration of protamine. Actually, the GIXOS signal of the monolayer after reaching the equilibrium has less pronounced features, which seem consistent with the loss of chain ordering observed by GIXD. On the other hand, the surface pressure does not change over time in the presence of Ca^{2+} ions (bright) even though the lateral pressure at $t=0$ is 10 mN m^{-1} smaller than that of Ca^{2+}-free subphase. The presence of 5 mM Ca^{2+} even seems sufficient to keep the LPS membrane intact against protamine (data not shown). This finding gives us clear evidence that the presence of Ca^{2+} is crucial for deep rough mutant bacteria to survive against lethal intruders. In fact, the GIXOS signals from the LPS Re monolayer on Ca^{2+}-loaded subphase can well be represented by the same slab model as the one used for the membranes before protamine injection.

Figures 8(B) and 8(C) show the MC simulations of the number densities $\Phi(z)$ of sugar moieties (LPS), Na^+ ions (Na), and Ca^{2+} ions (Ca) and the protamine (dark filled circles) for LPS Re monolayers on Ca^{2+}-free and Ca^{2+}-loaded subphases, respectively. Here, we assume a relatively high concentration of protamine (five molecules in a simulation volume). The corresponding instantaneous side views of the systems in the absence and presence of Ca^{2+} are presented in Figs. 8(D) and 8(E), respectively. In the absence of Ca^{2+} ions [Figs. 8(B) and 8(D)], positively charged protamine molecules strongly adsorb to the LPS Re membranes which leads to a suppression of the fluctuation of peptide chains. In fact, a distinct peak found inside the Kdo core region ($z \sim 5$ Å) indicates the intrusion of protamine into the membrane, which corresponds to a significant increase in the surface pressure [Fig. 8(A), dark]. In the presence of Ca^{2+} ions, protamine molecules are expelled from the deep core region [Fig. 8(C)]: the peak inside the Kdo core region ($z \sim 5$ Å) decreases and the peak corresponding to the protamine on the membrane surface ($z \sim 11$ Å) extends the tail toward the bulk. In fact, termini of loosely bound peptide chains can be identified in the instantaneous snapshot [Fig. 8(E)], which seems to account for the weaker interaction of protamine with the monolayer.

F. Role of Kdo cores in bacterial survival against protamine

In nature, it is known that lipid A is not sufficient for bacterial growth: both lipid A and two Kdo units are necessary for growth of most of gram negative bacteria under laboratory conditions [54,55] except for some unique examples. For instance, *Hemophilus influenzae* LPS has only one inner Kdo unit, but it has a phosphate group at the position where the carboxyl group of an outer Kdo is located [56]. The difference between lipid A and LPS Re is the charged Kdo moiety. Thus, to highlight the role of Kdo units in the survival of bacteria against protamine, we study the interaction of protamine with the monolayer of lipid A, prepared by acid hydrolysis of LPS Re. The pressure-area isotherms of lipid A monolayers on Ca^{2+}-free (dark) and Ca^{2+}-loaded subphases (bright) are presented in Fig. 9(A). In the presence of Ca^{2+}, the shoulder regime appears at lower surface pressure, suggesting that Ca^{2+} ions cause an increase in the lateral intermolecular interactions between lipid A molecules. The GIXOS results in the presence and absence of Ca^{2+} also show no significant difference (data not shown) compared to those of LPS Ra [17] and LPS Re (Fig. 1) due to its much more compact headgroup with no Kdo units.

When protamine solution is injected into the Ca^{2+}-free subphase after the compression of the monolayer up to π

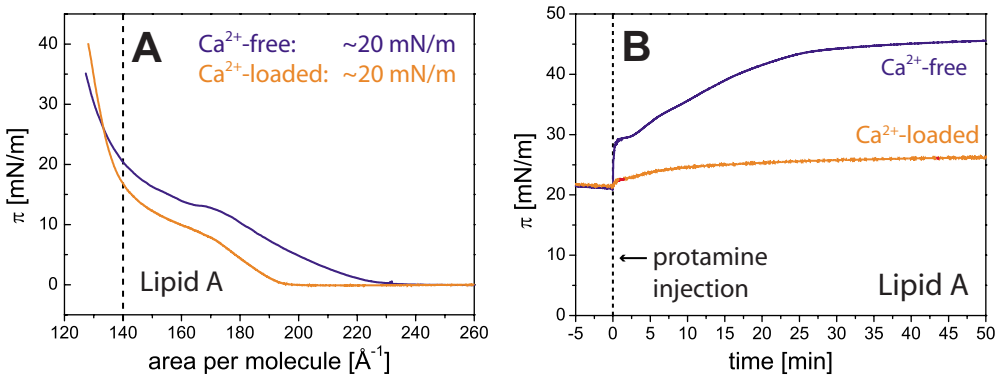

FIG. 9. (Color online) (A) Pressure-area isotherms of lipid A monolayers on Ca^{2+}-free subphase (dark) and Ca^{2+}-loaded subphase (bright). Grazing-incidence x-ray structural characterizations and protamine adsorption experiments (see below) are carried out at a constant area per molecule ($A=140$ Å^2, indicated with a broken line). (B) Surface pressure of lipid A monolayers plotted as a function of time on Ca^{2+}-free (dark) and Ca^{2+}-loaded (bright) buffers at $A=140$ Å^2. Protamine solution (final concentration of ~ 1 mg ml^{-1}) is injected at $t=0$. Note that there is a slight but distinct increase in the surface pressure even in the presence of Ca^{2+} (bright).

$=20$ mN m^{-1}, a significant increase in the surface pressure ($\Delta\pi \sim 25$ mN m^{-1}) can be observed [Fig. 9(B), dark], which is similar to the case of a LPS Re monolayer [Fig. 8(A)]. However, the lipid A monolayer does not stay fully intact against protamine even in the presence of Ca^{2+} [Fig. 9(B), bright]: the surface pressure increases slightly but monotonically upon the injection of protamine, resulting in $\Delta\pi \sim 5$ mN/m at $t=50$ min, suggesting a crucial role of the Kdo saccharides in the bacterial survival against protamine. It should be pointed out that GIXD results imply that hydrocarbon chains of lipid A take an ordered upright conformation (for detail, see the supplementary material [57]), which are almost identical to that of LPS Re (Fig. 4). In fact, the main phase transition temperatures of pentaacyl LPS or pentaacyl lipid A are approximately 15 °C lower than those of hexaacyl species [58]. Interestingly, Vaara and Nurminen [59] reported that pentaacyl and hexaacyl species show comparable MIC values against various antibiotics, suggesting that five hydrocarbon chains might be sufficient for the bacterial survival.

V. CONCLUSIONS

We combine the grazing incidence x-ray structural characterizations (GIXD and GIXOS) at the air/water interface and Monte Carlo simulations based on the minimal model to quantitatively determine the lateral ordering of hydrocarbon chains and the number or electron density perpendicular to the interface. The unique combination enables us to monitor the structures of the bacterial lipopolysaccharide (LPS) films in Å resolution with the minimal risk of radiation damages as well as to simulate the conformational changes of macromolecules (LPS and cationic peptides like protamine) occurring in 10^{-3} s. From the quantitative study on the minimal unit for the survival of bacteria (LPS Re) and the systematic comparison to lipid A lacking Kdo units, we conclude that the condensations of divalent ions (Ca^{2+} or Mg^{2+}) are crucial for bacteria to defend themselves against CAP intruders. Further studies that reveal the depth profiles of individual ion species, e.g., grazing incidence x-ray fluorescence, would be very helpful to gain deeper insight into the electrostatics of charged biological interfaces.

ACKNOWLEDGMENTS

M.T. thanks the German Science Foundation for support (Grant No. Ta 259/6). R.G.O. thanks Alexander von Humboldt Foundation and CONICET for support. E.S. thanks State Baden-Württemberg and DAAD for support. D.A.P. thanks the Natural Sciences and Engineering Research Council of Canada for support and C.B.H. thanks U.S. NSF (Grant No. DMR-0605652) for support. We also thank ESRF for synchrotron beam times, HPClab (St.F.X.U.) and ACENET for computing assistance, and the Advanced Foods and Materials Network of Centres of Excellence (AFMNet-NCE) and the Atlantic Innovation Fund for support.

APPENDIX: MINIMAL MODEL OF LATERAL CHAIN ORDERING

The hydrocarbon chain moiety is composed of six hydrocarbon chains in approximately two groups of three attached to a pair of glucosamines. Here we present a minimal model of the thermotropic phase transition of hydrocarbon chains. The intent is to discover (i) whether and to what extent the presence of Ca^{2+} ions will change the phase transition temperature an (ii) whether the presence of protamine, with and without Ca^{2+} ions, will bring about a change in that phase transition.

We considered the states of a single C12 hydrocarbon chain with an average long axis perpendicular to the local plane of the membrane and assumed the following: (a) no state that involves "doubling back" toward the air-water interface is included in the set of "allowed" chain conformations; (b) based on an assumption of approximately constant density of CH_2 and CH_3 groups, in common with experimental observations of phospholipid phase transitions, the cross-sectional area per chain projected onto the local membrane plane, with the chain possessing an extension ("length") L, is $A(L)=A_0L_0/L$, where L_0 is the extension length of the all-

trans chain and A_0 is the cross-sectional area when the chain is in an all-*trans* state with an extension L_0 [24,60]. A simple calculation yields $A_0 \sim 20$ Å^2 and $L_0=11$ in units of C—C bond length. Thus, a state with $L=8$ has cross-sectional area $A(8)=27.5$ Å^2, while one with $L=7$ has cross-sectional area $A(7)=31.4$ Å^2.

In accord with our pressure-area isotherms, we have considered LPS molecules with cross-sectional areas of ≤ 170 Å^2. The total areas of six hydrocarbon chain moieties packed onto a triangular lattice with molecular radii of 7 and 6 Å^2 are 169.7 and 124.7 Å^2, respectively. Accordingly, we restrict the set of allowed hydrocarbon chain states per chain to those with cross-sectional areas $A(L) \leq 169.7/6 = 28.3$ Å^2. This means that, in this model, we accept all states with L lying between 8 and 11 and ignore the remainder.

We then have 99 conformational states of a hydrocarbon chain possessing energies between 0 and $6E_{tg}$ and degeneracies between 1 and $(2)^6=64$, where E_{tg} is the *trans-gauche* energy difference, $E_{tg}=0.45\times 10^{-20}$ J. A rotation around the bond connecting two CH_2 groups on a chain exhibits one low-energy minimum (extended chain all-*trans* state at 0°) of energy 0 and two higher-energy minima (single *gauche* bond excited state at ±120°) of energy given by the *trans-gauche* energy, E_{tg} [60–63]. Recent simulation results [64] gave a value of $E_{tg}=0.37\times 10^{-20}$ J (0.54 kcal mol^{-1}), while the results of fitting calculated Raman spectra to experimental data [65] yielded $E_{tg}=0.56\times 10^{-20}$ J (0.80 kcal mol^{-1}). Early experiments [66,67] showed that the value of E_{tg} was approximately $(0.35-0.42)\times 10^{-20}$ J with a preference for the latter [66]. In accord with the two, more recent, values we chose the average, $E_{tg}\sim 0.45\times 10^{-20}$ J.

We divided these states into two sets, *s* and *b*—extended chain states with $L=10$ or 11 (*s*) and twisted chain states with $L=8$ or 9 (*b*)—and averaged over them using only the *trans-gauche* energy in the Boltzmann factor. We then obtained thermal averages of the internal energies and degeneracies for these two states, *s* and *b*, of a single hydrocarbon chain using the single-chain energies and degeneracies since we do not yet consider chain-chain interactions. Here,

$$E_s = \frac{E_{tg}[4\exp + 64\exp^2]}{Z_s}, \quad D_s = \frac{[1+(4)^2\exp+(32)^2\exp^2]}{Z_s}, \quad \text{where } Z_s = [1+4\exp+32\exp^2], \tag{A1}$$

$$E_b = \frac{E_{tg}[8\exp+80\exp^2+720\exp^3+1536\exp^4+2560\exp^5+1536\exp^6]}{Z_b}, \tag{A2}$$

$$D_b = \frac{[(8)^2\exp+(40)^2\exp^2+(240)^2\exp^3+(384)^2\exp^4+(512)^2\exp^5+(256)^2\exp^6]}{Z_b}, \tag{A3}$$

$$Z_b = [8\exp+40\exp^2+240\exp^3+384\exp^4+512\exp^5+256\exp^6], \tag{A4}$$

where $\exp \equiv \exp(-\beta E_{tg})$ with $\beta = 1/k_BT$ and k_B as Boltzmann's constant.

With six chains per molecule, the number of ways to distribute n chains ($n=0,1,\ldots,6$) in state *b* among six chains is ${}^6C_n$. This six-chain state possesses internal energy and degeneracy,

$$(6-n)E_s + nE_b = 6E_s + n(E_b - E_s), \tag{A5}$$

$$(D_b)^n(D_s)^{6-n} = (D_s)^6(D_b/D_s)^n. \tag{A6}$$

We should now treat these seven states as those of a six-chain hydrocarbon chain component. However, this might be unnecessary in this paper, that is, not primarily about hydrocarbon chain phase transitions but about protamine interacting with LPS Re headgroups and ions. Accordingly, we divide these seven states into two sets, *S* and *B*, where state *S* comprises the state with $n=0$ and state *B* is an average over the states $n=1,2,\ldots,6$ with

$$E_S = 6E_s, \quad D_S = (D_s)^6, \tag{A7}$$

$$E_B = \frac{\sum_{n=1}^{6} {}^6C_n[(6-n)E_s + nE_b](D_b)^n(D_s)^{6-n}}{\sum_{n=1}^{6} {}^6C_n(D_b)^n(D_s)^{6-n}} = \frac{6E_s\sum_{n=1}^{6} {}^6C_n n(E_b-E_s)(D_{rel})^n}{\sum_{n=1}^{6} {}^6C_n(D_{rel})^n}, \tag{A8}$$

$$D_B = \frac{\sum_{n=1}^{6}[{}^6C_n(D_b)^n(D_s)^{6-n}]^2}{\sum_{n=1}^{6} {}^6C_n(D_b)^n(D_s)^{6-n}} = \frac{(D_s)^6\sum_{n=1}^{6}[{}^6C_n(D_{rel})^n]^2}{\sum_{n=1}^{6} {}^6C_n(D_{rel})^n}, \tag{A9}$$

where ${}^6C_n = 6!/n!(6-n)!$ and $D_{rel}=D_b/D_s$. Thus, the free energies of these two states, i.e., the energy functions to be used in the MC simulations, are

$$F_S = E_S - k_BT\ell n(D_S) \quad \text{and} \quad F_B = E_B - k_BT\ell n(D_B). \tag{A10}$$

[1] K. Brandenburg, J. Andrä, M. Müller, M. H. J. Koch, and P. Garidel, Carbohydr. Res. **338**, 2477 (2003).

[2] R. E. W. Hancock and D. S. Chapple, Antimicrob. Agents Chemother. **43**, 1317 (1999).

[3] T. D. Brock, Can. J. Microbiol. **4**, 65 (1958).

[4] L. T. Hansen, J. W. Austin, and T. A. Gill, Int. J. Food Microbiol. **66**, 149 (2001).

[5] N. M. Islam, T. Itakura, and T. Motohiro, Bull. Jpn. Soc. Sci. Fish. **50**, 1705 (1984).

[6] P. Pincus, Macromolecules **24**, 2912 (1991).

[7] E. B. Zhulina, J. Klein Wolterink, and O. V. Borisov, Macromolecules **33**, 4945 (2000).

[8] N. A. Kumar and C. Seidel, Macromolecules **38**, 9341 (2005).

[9] A. Naji, C. Seidel, and R. R. Netz, in *Surface-Initiated Polymerization II*, edited by K.-S. Lee *et al.* (Springer, Berlin, 2006).

[10] S. Pal and C. Seidel, Macromol. Theory Simul. **15**, 668 (2006).

[11] N. A. Kumar and C. Seidel, Phys. Rev. E **76**, 020801(R) (2007).

[12] O. J. Hehmeyer, G. Arya, A. Z. Panagiotopoulos, and I. Szleifer, J. Chem. Phys. **126**, 244902 (2007).

[13] L. P. Kotra, D. Golemi, N. A. Amro, G. Y. Liu, and S. Mobashery, J. Am. Chem. Soc. **121**, 8707 (1999).

[14] R. D. Lins and T. P. Straatsma, Biophys. J. **81**, 1037 (2001).

[15] R. M. Shroll and T. P. Straatsma, Biopolymers **65**, 395 (2002).

[16] D. A. Pink, L. T. Hansen, T. A. Gill, B. E. Quinn, M. H. Jericho, and T. J. Beveridge, Langmuir **19**, 8852 (2003).

[17] R. G. Oliveira, E. Schneck, B. Quinn, O. Konovalov, T. Gill, C. Hanna, D. A. Pink, and M. Tanaka, C. R. Chim. **12**, 209 (2009).

[18] S. Mora, J. Daillant, D. Luzet, and B. Struth, Europhys. Lett. **66**, 694 (2004).

[19] C. Galanos, O. Lüderitz, and O. Westphal, Eur. J. Biochem. **9**, 245 (1969).

[20] K. Brandenburg and U. Seydel, Biochim. Biophys. Acta **775**, 225 (1984).

[21] K. Kjaer, J. Als-Nielsen, C. A. Helm, L. A. Laxhuber, and H. Möhwald, Phys. Rev. Lett. **58**, 2224 (1987).

[22] V. D. Jacquemain, S. G. Wolf, F. Leveiler, M. Deutsch, K. Kjaer, J. Als-Nielsen, M. Lahav, and L. Leiserowitz, Angew. Chem. **104**, 134 (1992).

[23] S. Doniach, J. Chem. Phys. **68**, 4912 (1978).

[24] D. A. Pink, T. J. Green, and D. Chapman, Biochemistry **19**, 349 (1980).

[25] O. G. Mouritsen, A. Boothroyd, R. Harris, N. Jan, T. Lookman, L. MacDonald, D. A. Pink, and M. J. Zuckermann, J. Chem. Phys. **79**, 2027 (1983).

[26] A. Caille, D. Pink, F. de Verteuil, and M. J. Zuckermann, Can. J. Phys. **58**, 581 (1980).

[27] E. T. Rietschel *et al.*, in *Handbook of Endotoxin*, edited by E. T. Rietschel (Elsevier, Amsterdam, 1984), Vol. 1, p. 187.

[28] T. A. Gill, D. S. Singer, and J. W. Thompson, Process Biochem. (Oxford, U.K.) **41**, 1875 (2006).

[29] D. M. Smilgies, N. Boudet, B. Struth, and O. Konovalov, J. Synchrotron Radiat. **12**, 329 (2005).

[30] J. Als-Nielsen and D. McMorrow, *Elements of Modern X-Ray Physics* (Wiley, New York, 2001).

[31] K. Kjaer, J. Alsnielsen, C. A. Helm, P. Tippmankrayer, and H. Mohwald, J. Phys. Chem. **93**, 3200 (1989).

[32] V. M. Kaganer, I. R. Peterson, R. M. Kenn, M. C. Shih, M. Durbin, and P. Dutta, J. Chem. Phys. **102**, 9412 (1995).

[33] J. N. Israelachvili, *Intermolecular and Surface Forces* (Academic Press, London, 1991).

[34] M. Hermansson, Colloids Surf., B **14**, 105 (1999).

[35] S. L. Walker, J. A. Redman, and M. Elimelech, Langmuir **20**, 7736 (2004).

[36] V. Vlachy, Annu. Rev. Phys. Chem. **50**, 145 (1999).

[37] A. Chakrabarti, P. Nelson, and R. Toral, J. Chem. Phys. **100**, 748 (1994).

[38] I. Carmesin and K. Kremer, Macromolecules **21**, 2819 (1988).

[39] C. Fleck, R. R. Netz, and H. H. von Grünberg, Biophys. J. **82**, 76 (2002).

[40] D. A. Pink, M. Belaya, V. Levadny, and B. Quinn, Langmuir **13**, 1701 (1997).

[41] M. Deserno, C. Holm, and S. May, Macromolecules **33**, 199 (2000).

[42] D. A. Pink, C. B. Hanna, B. E. Quinn, V. Levadny, G. L. Ryan, L. Filion, and A. T. Paulson, Food Res. Int. **39**, 1031 (2006).

[43] R. R. Netz, Phys. Rev. E **60**, 3174 (1999).

[44] R. R. Netz and D. Andelman, Phys. Rep. **380**, 1 (2003).

[45] P. Y. Lai and K. Binder, J. Chem. Phys. **97**, 586 (1992).

[46] K. Binder, *Monte Carlo Simulation in Statistical Physics: An Introduction* (Springer, Berlin, 1988).

[47] K. Brandenburg, M. H. J. Koch, and U. Seydel, Eur. J. Biochem. **258**, 686 (1998).

[48] E. Blatt and W. L. C. Vaz, Chem. Phys. Lipids **41**, 183 (1986).

[49] P. Garidel, M. Rappolt, A. B. Schromm, J. Howe, K. Lohner, J. Andrä, M. H. J. Koch, and K. Brandenburg, Biochim. Biophys. Acta **1715**, 122 (2005).

[50] C. A. Helm, P. Tippmannkrayer, H. Mohwald, J. Alsnielsen, and K. Kjaer, Biophys. J. **60**, 1457 (1991).

[51] W. H. Press, S. A. Teukolsky, W. T. Vetterling, and B. P. Flannery, *Numerical Recipes in C* (Cambridge University Press, Cambridge, 1992).

[52] R. Potter, L. Truelstrup Hansen, and T. Gill, Int. J. Food Microbiol. **103**, 23 (2005).

[53] L. A. Glaser, A. T. Paulson, R. A. Speers, R. Y. Yada, and D. Rousseau, Food Hydrocolloids **21**, 495 (2007).

[54] C. R. Raetz, J. Bacteriol. **175**, 5745 (1993).

[55] *Escherichia Coli and Salmonella Typhimurium*, edited by H. Nikaido and M. Vaara (ASM, Washington, D.C., 1987).

[56] N. J. Phillips, M. A. Apicella, J. M. Griffiss, and B. W. Gibson, Biochemistry **31**, 4515 (1992).

[57] See supplementary material at http://link.aps.org/supplemental/10.1103/PhysRevE.81.041901 for a GIXD reciprocal space map of a lipid A monolayer on Ca^{2+}-loaded buffer.

[58] K. Brandenburg, S. Kusumoto, and U. Seydel, Biochim. Biophys. Acta **1329**, 183 (1997).

[59] M. Vaara and M. Nurminen, Antimicrob. Agents Chemother. **43**, 1459 (1999).

[60] G. Cevc and D. Marsh, *Phospholipid Bilayers: Physical Principles and Models* (Wiley, Toronto, 1987).

[61] J. Zheng, K. Kwak, J. Xie, and M. D. Fayer, Science **313**, 1951 (2006).

[62] R. M. Venable, Y. Zhang, B. J. Hardy, and R. W. Pastor, Science **262**, 223 (1993).

[63] P. Meier, J. H. Sachse, P. J. Brophy, D. Marsh, and G. Kothe, Proc. Natl. Acad. Sci. U.S.A. **84**, 3704 (1987).
[64] J. B. Klauda, R. W. Pastor, and B. R. Brooks, J. Phys. Chem. B **109**, 15684 (2005).
[65] R. G. Snyder, J. Chem. Soc., Faraday Trans. **88**, 1823 (1992).
[66] L. S. Bartell and D. A. Kohl, J. Chem. Phys. **39**, 3097 (1963).
[67] A. Abe, R. L. Jernigan, and P. J. Flory, J. Am. Chem. Soc. **88**, 631 (1966).